A Broadband Implantable and a Dual-Band On-Body Repeater Antenna: Design and Transmission Performance

Asimina Kiourti, *Member, IEEE*, Jorge R. Costa, *Senior Member, IEEE*, Carlos A. Fernandes, *Senior Member, IEEE*, Konstantina S. Nikita, *Senior Member, IEEE*

***Abstract*—The design of a new miniature broadband implantable antenna and a dual–band on–body antenna are presented along with the transmission performance between the two. The former and latter antennas are intended for integration into implantable medical devices (IMDs) and on–body repeaters, respectively. The on–body repeater antenna favors the use of very low power IMDs. The on–body repeater receives low power data from an IMD (MedRadio band, 401–406 MHz) and retransmits it to remote devices placed further apart (ISM band, 2400–2480 MHz). The MedRadio implantable antenna maintains miniature size (399 mm^3), and exhibits two close resonances which increase the –10 dB bandwidth inside muscle tissue (87 MHz). The on–body antenna is relatively small (6720 mm^3), and exhibits dual resonances in the MedRadio and ISM bands. Assuming a typical arm implantation scenario and an on–body receiver sensitivity of –75 dBm, the proposed configuration is found to enable reduction of the IMD power by a factor of 100. Patient safety and tolerance to electromagnetic interference are, thus, preserved, and lifetime of the IMD is increased. The set–up is, finally, shown to be robust to antenna misalignment and polarization rotation.**

***Index Terms*—Implantable antenna, medical device radiocommunications services, phantom, repeater antenna, telemetry, transmission coefficient.**

I. Introduction

IMPLANTABLE medical devices (IMDs) may be used as measurement/control devices (e.g., sensors, drug infusion devices, artificial organ controls) or stimulators (e.g., pacemakers, neurostimulators, pain suppression devices, cochlear implants), and are recently attracting significant scientific interest for a number of diagnostic and therapeutic applications [1]–[3]. One of the most crucial aspects of IMDs is their ability to wirelessly communicate with exterior equipment for monitoring/control purposes. This necessitates the design of implantable and exterior antennas for integration into IMDs and exterior monitoring/control equipment, respectively. Wireless telemetry for IMDs is most commonly performed in the low–frequency band of 401–406 MHz, which has been exclusively allocated for Medical Device Radiocommunications (MedRadio) services [4]. Apart from being internationally available, the MedRadio band allows for acceptable propagation through human tissue, falls within a relatively low noise portion of the spectrum, and is feasible with low power circuits.

One of the major challenges of implantable antenna design is to achieve a wide –10 dB bandwidth (BW_{10dB}), while still maintaining miniature size and adequate radiation performance. Inter–subject variations in anatomical structure and tissue electrical properties [5], as well as fabrication and testing inaccuracies [6], have the potential to detune the antenna. In the literature, wideband MedRadio antennas have been proposed for implantation inside the skin (BW_{10dB} = 82 MHz) [7] and muscle (BW_{10dB} = 97 MHz) [8]. However, they exhibit relatively increased size (1266 and 791 mm^3, respectively), for the sake of improved radiation performance (maximum far–field gains inside the tissue models under consideration, G_{max}, of –25 and –27 dBi, respectively). A miniature (122 mm^3), yet wideband (BW_{10dB} = 122 MHz) MedRadio implantable antenna has also been presented [9]. However, it exhibits poor radiation performance (G_{max} = –38 dBi), as attributed to its small radiating surface. Furthermore, all aforementioned antennas exhibit rectangular shape, and, thus, sharp edges, which may traumatize biological tissues in case they are directly exposed to the surrounding tissue environment, rather than integrated within the IMD [10]. To address this issue, conformal [11], [12] and circular [6] designs have been reported for implantable antennas.

Given the requirement for miniaturization, MedRadio implantable antennas exhibit very low radiation efficiencies (usually less than 1%) [13]. Moreover, the maximum power incident to an implantable antenna is restricted by patient safety (e.g., IEEE C95.1–1999 [14] and IEEE C95.1–2005 [15]) and electromagnetic (EM) interference [4] regulations. Therefore, in order to achieve increased telemetry ranges (e.g.

Manuscript received May 27, 2013, revised January 28, 2014, accepted March 01, 2014. This work was supported by the COST VISTA (IC1102) Action, and the Operational Program "Education and Lifelong Learning", co-financed by the European Union and Greek national funds, under the project ARISTEIA DEM-II-MED. The work of A.K. was supported by the IEEE MTT-S Graduate Fellowship for Medical Applications.

A. Kiourti and K.S. Nikita are with the School of Electrical and Computer Engineering, National Technical University of Athens, Athens 15780, Greece (e-mail: akiourti@biosim.ntua.gr, knikita@ece.ntua.gr).

J.R. Costa is with Instituto de Telecomunicações and Departamento de Ciências e Tecnologias da Informação, Instituto Universitario de Lisboa (ISCTE-IUL), Lisboa 1649-026, Portugal (e-mail: Jorge.Costa@lx.it.pt).

C.A. Fernandes is with Instituto de Telecomunicações and Instituto Superior Técnico, University of Lisbon, Lisboa 1049-001, Portugal (e-mail: carlos.fernandes@lx.it.pt).

total of 5 m [16], [17] or 6 m [18]), the implant must be operated at its maximum allowable transmit power levels. This, in turn, implies a fast battery drain for the IMD. Numerical transmission coefficient ($|S_{21}|$) investigations between MedRadio implantable and dipole antennas have been performed in [6], [16]. Experimental $|S_{21}|$ investigations have been performed at 402 MHz between implantable and exterior loop antennas [19], and at 2450 MHz between implantable and commercial chip antennas [20]. Numerical and experimental $|S_{21}|$ investigations between MedRadio implantable and sophisticated miniature on–body antennas have not been reported in the literature.

In this study, we suggest the use of an on–body repeater which receives signals from the IMD and further retransmits them to exterior monitoring/control devices. The repeater aims to extend the IMD telemetry range by receiving weak signals from the IMD (MedRadio band, 401–406 MHz), and retransmitting them to exterior devices placed further apart (Industrial Scientific and Medical, ISM, band, 2400–2480 MHz [21]). The high–frequency ISM band allows for the design of efficient, yet small enough, antennas, which are adequate for on–body usage. Another advantage of this relay configuration is that lower power levels are required for the implantable antenna, which assist in: (a) preserving patient safety against radiated EM fields, (b) eliminating EM interference, and (c) increasing the lifetime of the IMD.

The first challenge lies in designing and testing a novel MedRadio antenna for muscle–implantation. Compared to previous designs, the proposed antenna shows improved tolerance to detuning, by exhibiting an enhanced –15 dB impedance bandwidth (BW_{15dB}), further to its BW_{10dB}. This is a strongly desired property for implantable antennas which are intended to operate inside unpredictable tissue environments (electrical properties and geometry). Emphasis is also given in preserving patient comfort, by introducing a circular shape to avoid sharp edges, and miniaturizing its size. To assist in experimental testing, a liquid muscle–equivalent phantom is formulated in the MedRadio band. The second challenge lies in designing and testing a novel miniature dual–band (402, 2400 MHz) on–body antenna. It is highlighted that, apart from some preliminary recent work found in [22], no other on–body antenna has been reported in the literature for dual–operation in these bands. The last challenge lies in numerically and experimentally investigating the transmission performance between these antennas, and, therefore, the relay concept feasibility. The goal is to assess the lowest power incident to the implantable antenna which achieves reliable data telemetry for a typical medical implantation scenario. Antenna polarization and misalignment issues are also addressed, while transmission of real data is demonstrated.

The paper is organized as follows. Section II describes the numerical method used in this study. Section III assesses the formulation of the muscle–equivalent phantom. Design and testing of the proposed implantable and on–body repeater antennas are provided in Sections IV and V, respectively. Transmission performance investigations are carried out in Section VI. The paper concludes in Section VII.

TABLE I
RECIPE FOR MUSCLE–EQUIVALENT PHANTOM IN THE MEDRADIO BAND

Ingredients	Percentage Contribution(*)
Deionized water	47.62%
Glycerol	50.81%
NaCl	1.57%

(*) measured permittivity = 58.0, measured conductivity = 0.8 S/m

II. NUMERICAL METHOD

Finite Element (FE) simulations are carried out using the commercial software Ansoft HFSS [23]. The FE solver performs tetrahedron–meshing of the geometry in an iterative way, with the mesh being automatically perturbed by 30% between each pass. The refinement procedure stops when the maximum change in the reflection coefficient magnitude ($|S_{11}|$) between two consecutive passes is less than 0.02 or when the number of passes exceeds 15. Single–frequency simulations are performed at 402 MHz, whereas broadband simulations are performed by means of a 400 point frequency sweep inside a ±100 MHz range around 402 MHz. Absorbing boundaries are set $\lambda_0/4$ (λ_0 is the free–space wavelength at 402 MHz) away from all simulation set–ups. The goal is to take free–space radiation into account and extend radiation infinitely far, while guaranteeing stability of the numerical calculations [23].

III. MUSCLE-EQUIVALENT PHANTOM FORMULATION

Experimental investigations are carried out inside a liquid muscle phantom, which is simple to form and nearly equivalent to multi–layer phantoms for implantable antenna design and performance investigation [24]. A recipe is formulated for a MedRadio muscle–equivalent phantom in liquid state, as indicated in Table 1. In the literature, there exist some muscle–equivalent phantoms [25], [26]. As part of this study, we adapted the mixture to obtain the required electrical properties using only the ingredients shown in Table 1. Deionized water acts as the base. Addition of glycerol reduces permittivity (ε_r), without affecting conductivity (σ). Salt increases σ, and, slightly, increases ε_r [7].

Electrical properties of the phantom are obtained from the scattering matrix of an in-house developed sample holder, measured using a Vector Network Analyzer (VNA). The complex permittivity is de–embedded using a technique developed by the authors, presented in [27]. The technique is based on reflection (S_{11}) and transmission (S_{21}) coefficient measurements of a parallelepiped container intercepted by the inner conductor of a coaxial cable. For example, Fig. 1(a) shows the container filled with the liquid muscle–equivalent phantom. The transfer function between the two coaxial connectors outside the container depends upon the electrical properties of the container's filling material. This can be de–embedded by comparing measurement with simulation results for the same structure. The measurement set–up is shown in Fig. 1(b). We highlight that the most common technique for obtaining the complex permittivity of a dielectric material consists of measuring the complex reflection coefficient [28]. In this work, we move the idea even further to apply a transmission method which involves measurement of all complex scattering parameters. As has been noted in [29], the

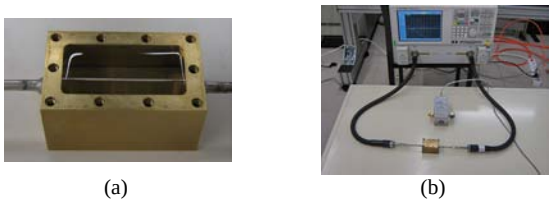

(a) (b)

Fig. 1. MedRadio muscle–equivalent phantom: (a) coaxial container for complex permittivity measurement, and (b) experimental set–up used for measuring the phantom electrical properties.

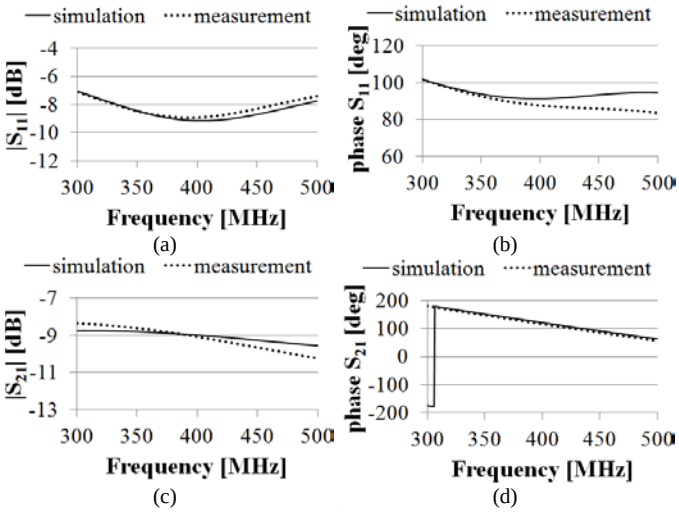

Fig. 2. Electrical properties results for the MedRadio muscle–equivalent phantom (simulations are for ε_r = 58.0, σ = 0.8 S/m): (a) reflection coefficient magnitude ($|S_{11}|$), (b) reflection coefficient phase (phase S_{11}), (c) transmission coefficient magnitude ($|S_{21}|$), and (d) transmission coefficient phase (phase S_{21}).

relevant scattering parameters relate closely to the complex permittivity of the material under test. For example, relative permittivity of biological media has recently been computed as a linear sum of a measured set of scattering parameters [30]. Based on the above, the scattering parameters of the coaxial container shown in Fig. 1 uniquely characterize the enclosed phantom material, and can, therefore, be considered as an equivalent representation of its complex permittivity.

Numerical and experimental results regarding the electrical properties assessment of the phantom are superimposed in Fig. 2. Quite good agreement is observed at 402 MHz for ε_r = 58.0 and σ = 0.8 S/m. These compare well with the theoretical electrical properties of muscle tissue at 402 MHz (ε_r = 57.1, σ = 0.8 S/m [31]). Deviations between numerical and experimental results at frequencies other that 402 MHz are attributed to the frequency dependency of the phantom's electrical properties. Analytically solving the EM structure of Fig. 1 is an ongoing research topic, which aims to directly translate the measured S–parameters into the complex permittivity values of the phantom under consideration, but this is out of the scope of this paper.

IV. Broadband Implantable Antenna

A. Antenna Design

A parametric model of a broadband patch antenna is proposed for muscle–implantation and telemetry in the MedRadio band, as shown in Fig. 3(a)–(c) (e.g., glucose or pressure monitoring etc). The antenna structure is circular

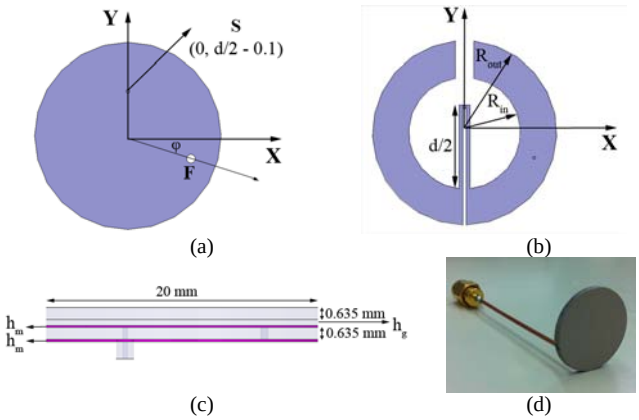

Fig. 3. Proposed broadband implantable antenna: (a) ground plane, (b) patch plane, (c) side view, and (d) fabricated prototype.

(radius of R = 10 mm), and includes ground and patch planes printed on 0.635 mm–thick Rogers RO 3210 dielectric material (permittivity, ε_{rd} = 10.2, loss tangent, tanδ = 0.003). Size of the antenna is selected as a compromise between miniaturization and exhibited radiation performance, as indicated by the authors in [32]. Origin of the coordinate system is located at the center of the ground plane, according to Fig. 3(a). The patch has a ring shape (outer radius of R_{out}, inner radius of R_{in}), with a 2 mm–wide rectangular part removed from one side (+y axis), and a (d + 1.2 mm)–long meandered path added on the opposite side (–y axis). Copper sheets with a thickness of h_m are considered for the ground and patch planes. The structure is fed by a 50 Ohm EZ–47 coaxial cable, placed at F: $((R_{in} + R_{out}/2)*\cos\varphi, -(R_{in} + R_{out}/2)*\sin\varphi)$. A 0.1 mm–radius shorting pin, placed at S: (0 mm, d/2 – 0.1 mm), connects the patch to the ground plane for miniaturization purposes [33]. A 0.635 mm–thick Rogers RO 3210 superstrate covers the structure to ensure biocompatibility. Glue (permittivity of ε_{rg}, thickness of h_g) is used to bond the dielectric layers together. The importance of simulating the presence of glue in multi–layered implantable antennas has been demonstrated in [34]. The parametric model is designed to excite two close resonances around the MedRadio band, which help achieve a wide resonance bandwidth for the antenna. More specifically, the current path from the shorting pin (S) to the right end of the ring–shaped patch (the one that passes through the +x axis) excites a resonance at a frequency higher than 402 MHz, while the current path from the feed point (F) to the left end of the ring–shaped patch (the one that passes through the –x axis) excites a resonance at a frequency lower than 402 MHz. Compared to our previous implantable antenna design reported in [6], the proposed antenna exhibits relatively increased occupied volume (399 mm^3 vs 204 mm^3 [6]), in favor of enhanced BW_{10dB} (87 MHz), BW_{15dB} (66 MHz), and G_{max} (–31 dBi). Size versus performance considerations for implantable antennas have been discussed in [32], [33].

Regarding the biocompatibility of the proposed antenna design, two issues need to be highlighted. Firstly, Rogers RO 3210 (ε_{rd} = 10.2, tanδ = 0.003) has been selected because of its availability in our lab, and its similar electrical properties to biocompatible ceramic alumina (ε_{rd} = 9.6, tanδ = $3\cdot10^{-5}$), which has been long used in medical implants [35]. Secondly, in the current set–up, the antenna ground plane is considered

to be in direct contact with the surrounding biological tissues. Even though copper is a non–biocompatible material, this approach has been adopted as a proof of concept for the resonance and radiation performance exhibited by the antenna, as has been the case in [6], [7]. Nevertheless, the ground plane can easily be plated with a biocompatible metal, or hidden by a very thin layer of biocompatible dielectric. In a realistic scenario, the antenna might be integrated into a biocompatible IMD which will also serve as its ground plane, or it might be included within the IMD's biocompatible case. In such scenarios, the modification of the antenna surrounding does not imply a change of the antenna design and concept, but rather a tuning of its parameters [36].

As part of this study, fine–tuning of the antenna design is performed inside the tissue–box of Fig. 4(a), which simulates muscle tissue at 402 MHz (ε_r = 57.1, σ = 0.8 S/m [31]). This tissue–box has been shown to achieve accelerated and optimized design for implantable antennas, regardless of the specific medical application scenario under consideration (e.g., implantation inside the muscle tissue of the human arm or the human trunk etc) [24]. The antenna is placed inside the box so that the coordinate systems of Fig. 3(a) and Fig. 4(a) coincide. Size of the box is determined by the antenna dimensions (R = 10 mm is the radius of the antenna), and the actual air–to–antenna separation distance for a typical muscle implantation scenario (h = 10 mm). For example, if h_m and h_g are to be ignored, for simplicity purposes, then the design parameters of Table II ("simplified antenna") are found to achieve the desired resonance characteristics. The reflection coefficient frequency response of the "simplified antenna" is shown in Fig. 5.

As compared to previously reported broadband implantable antennas, the proposed "simplified antenna" exhibits the following advantages: (a) increased tolerance to detuning phenomena caused by inter–subject variability, fabrication and testing inaccuracies, etc (BW_{15dB} = 66 MHz, BW_{10dB} = 87 MHz MHz), (b) implant–friendly shape (circular), and (c) good compromise between size (399 mm^3), bandwidth and achieved radiation performance (G_{max} = –31 dBi). All aforementioned performance parameters have been evaluated for the simulation set–up of Fig. 4(a). Furthermore, the proposed parametric antenna model: (a) increases flexibility in design thanks to the high number of variable parameters or, equivalently, degrees of freedom, and (b) includes a glue–layer which allows fine–tuning of the antenna at the fabrication step.

B. Sensitivity Tests and Measurement Results

A prototype of the proposed implantable antenna is fabricated and tested. Initially, fabrication–specific considerations are addressed, as imposed by the available pre–metalized substrate (h_m) and glue (h_g and ε_{rg}) materials. The design parameters of Table II ("to–be–fabricated antenna") are found to fine–tune the antenna in this case. Glue parameters (h_g and ε_{rg}) are set to values found through previous experience. The occurring reflection coefficient frequency response is shown in Fig. 5 ("to–be–fabricated antenna").

Sensitivity tests are further performed, which aim to assess antenna tolerance to the most sensitive experimental factors, as determined by the authors in [27]. Fig. 6 shows the

(a) (b)

Fig. 4. Tissue models used for implantable antenna design and testing: (a) numerical model, and (b) experimental phantom.

TABLE II
VARIABLE VALUES OF THE PARAMETRIC IMPLANTABLE ANTENNA MODEL

	simplified antenna	to–be–fabricated antenna
h_m	0 mm	0.035 mm
ε_{rg}	–	4.5
h_g	0 mm	0.08 mm
φ	20 deg	25 deg
R_{out}	9.9 mm	9.9 mm
R_{in}	4.5 mm	4.3 mm
d	18.9 mm	20.1 mm

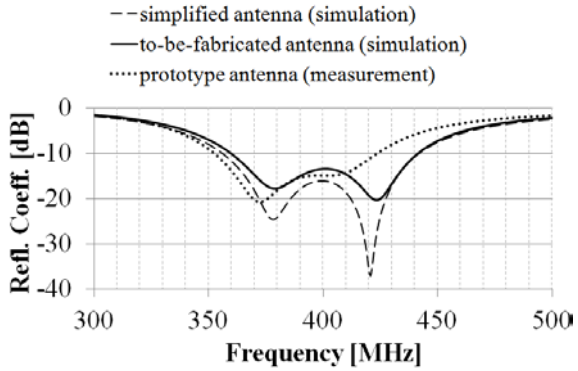

Fig. 5. Reflection coefficient frequency response of the proposed broadband implantable antenna.

deviation of the original antenna's reflection coefficient frequency response to changes in: (a) glue permittivity, ε_{rg} (Fig. 6(a)), (b) thickness of glue, h_g (Fig. 6(b)), (c) radius of the antenna, R (Fig. 6(c)), (d) permittivity of Rogers RO 3210, ε_{rd} (Fig. 6(d)), (e) phantom permittivity, ε_{rph} (Fig. 6(e)), and (f) phantom conductivity, σ_{ph} (Fig. 6(f)). Percent deviations of the center resonance frequency (f_c), average reflection coefficient within the bandwidth ($|S_{11}|_{@BW}$), and –10 dB bandwidth (BW_{10dB}) are found to range in the [–2.3%, +2.8%], [–28.6%, +23.6%], and [–8.4%, +7.2%] intervals, respectively. However, the antenna resonance performance is found to be adequate in the MedRadio band ($|S_{11}|_{@MedRadio}$ < –10 dB) for all these scenarios, thus, highlighting its tolerance to detuning phenomena caused by fabrication and testing inaccuracies.

An antenna prototype is then fabricated, using photolithography (Fig. 3(d)). The prototype is placed at a distance of h = 10 mm under the side surface of a typical drinking plastic cup (lower diameter of 55 mm, upper diameter of 75 mm, height of 110 mm) (Fig. 4(b)), semi–filled with the muscle–equivalent phantom that was formulated in Section III. The aim is to emulate the muscle tissue simulating box of Fig. 4(a), by taking into account the fact that the exact shape of the surrounding tissue does not influence the experimental results. The reflection coefficient frequency response of the antenna is measured with a VNA, and is super–imposed in Fig. 5 ("prototype antenna"). Good

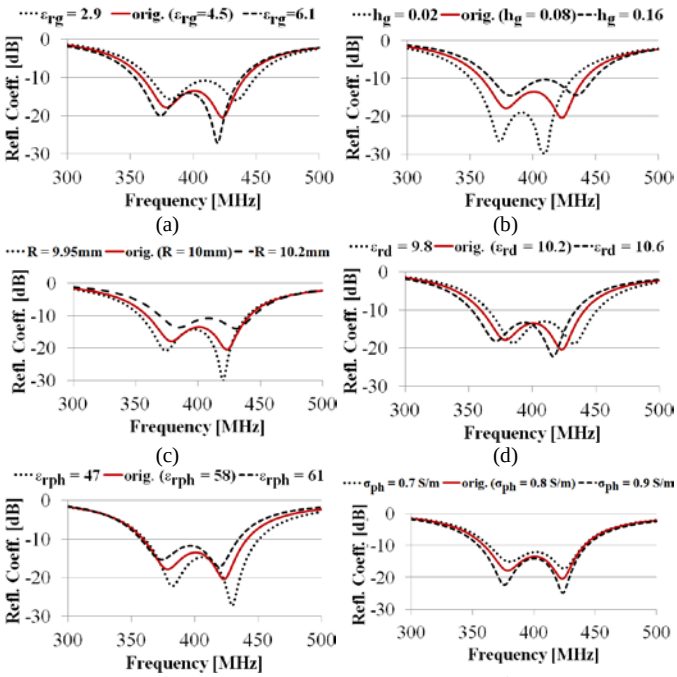

Fig. 6. Sensitivity tests of the proposed broadband implantable antenna to changes in: (a) permittivity of glue (ε_{rg}), (b) thickness of glue (h_g), (c) radius of the antenna (R), (d) permittivity of Rogers RO 3210 (ε_{rd}), (e) phantom permittivity (ε_{rph}), and (f) phantom conductivity (σ_{ph}).

agreement exists between numerical ("to–be–fabricated antenna") and experimental ("prototype antenna") results. Recorded percent deviations of f_c, $|S_{11}|_{@BW}$, and BW_{10dB} equal –2.0%, +20.2%, and –8.4%, respectively, which lie within the aforementioned expected intervals of uncertainty.

It is worth noting that the feeding coaxial cable used in the simulations (Fig. 3(c)) and measurements (Fig. 3(d)) is having a negligible effect on the antenna performance. As a proof of concept, Fig. 7 super–imposes numerical results for different lengths of coaxial cables, along with results for the case where the coaxial cable feed is replaced by a discrete port. This has further been verified through simulations and measurements of the antenna performance at different insertion depths within the phantom (a reduced insertion depth frees the cable from the phantom [11]). Results are attributed to the fact that the antenna ground plane is in direct contact with the phantom, so that the high losses of the equivalent biological tissues attenuate the currents on the ground plane and prevent their flow on the cable [37].

V. Dual–Band On–Body Repeater Antenna

A. Antenna Design

A dual–band patch antenna is proposed for integration into on–body repeater devices which are intended to extend the communication range of IMDs by receiving their weak signals (MedRadio band, 401–406 MHz) and re–transmitting them to monitoring/control devices placed further apart (ISM band, 2400–2480 MHz). Apart from some preliminary recent work found in [22], no other on–body antenna has been reported in the literature for dual–operation in these bands. The numerical antenna model is shown in Fig. 8(a). The geometry exhibits rectangular shape (60 mm × 70 mm), and consists of

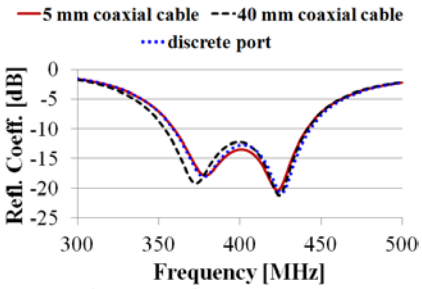

Fig. 7. Resonance performance of the implantable antenna considering different feeds, showing that the coaxial cable is having a negligible effect.

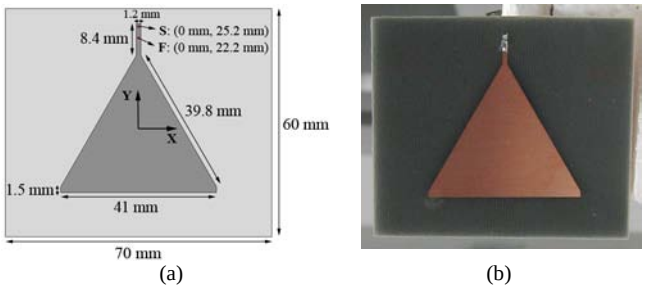

Fig. 8. Proposed dual–band on–body repeater antenna: (a) numerical model, and (b) fabricated prototype.

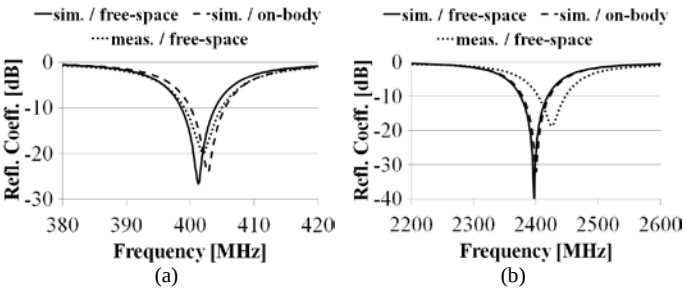

Fig. 9. Reflection coefficient frequency response of the proposed dual–band on–body repeater antenna around the: (a) MICS, and (b) ISM bands.

rectangular ground and triangular patch planes printed on 1.6 mm–thick FR4 dielectric material (ε_r = 4.4, tanδ = 0.02). Origin of the coordinate system is located at the center of the rectangular ground plane. In order to excite dual resonances, the shape of the triangular patch is modified to include two conductive rectangles on its top vertex (length of 8.4 mm, width of 1.2 mm) and bottom side (length of 41 mm, width of 1.5 mm), while a shorting pin is inserted at S: (0 mm, 5.2 mm) to connect the ground and patch planes. The structure is fed by a 50 Ohm EZ–86 coaxial cable, placed at F: (0 mm, 22.2 mm).

The numerical reflection coefficient frequency response of the antenna around the MedRadio and ISM bands is shown in Fig. 9(a) and Fig. 9(b), respectively. Simulations have been carried out considering the antenna: (a) in free–space ("sim. / free–space"), and (b) at a distance of 15 mm from a 300 mm × 300 mm × 70 mm block of muscle tissue (to mimic the presence of clothes) ("sim. / on–body"). Numerical results in these two cases are almost identical, indicating that the exhibited resonance performance is not affected by the presence of biological tissues in close proximity. Dual resonances are excited at 402 and 2400 MHz, which exhibit BW_{10dB} values of 6 MHz and 45 MHz, respectively.

Current distributions on the patch surface at these frequencies are shown in Fig. 10(a) (antenna in free–space)

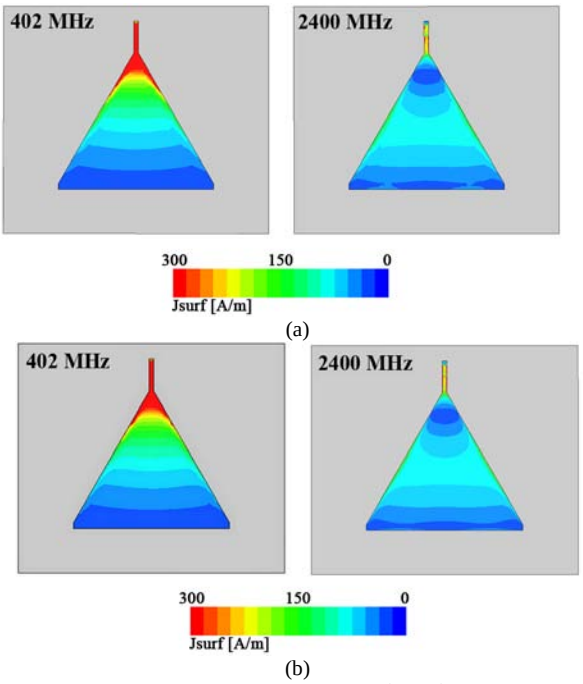

Fig. 10. Current distributions on the patch surface of the on–body repeater antenna when placed: (a) in free–space, and (b) at a distance of 15 mm from a 300 mm × 300 mm × 70 mm block of muscle tissue.

and Fig. 10(b) (antenna at 15 mm distance from the 300 mm × 300 mm × 70 mm block of muscle tissue). At 402 MHz, high currents are excited around the shorting pin and the conductive rectangle which has been added on the top vertex of the triangular patch. At 2400 MHz, the current is more evenly distributed within the surface of the patch. Nearly no change is induced in the current patterns by the presence of human tissue at a close distance (15 mm).

B. Sensitivity Tests and Measurement Results

A prototype of the proposed dual–band on–body antenna is fabricated and measured. Initially, sensitivity tests are performed, which aim to assess antenna tolerance to the most sensitive fabrication factors, i.e. positioning of the coaxial feed (F) and shorting pin (S), and permittivity of the substrate material. Changes in the y coordinate of F and S within the [23.7 mm, 25.7 mm] and [20.2 mm, 22.8 mm] intervals, respectively, and changes in the FR4 permittivity by ±4% are found to alter the original resonance frequency around the MedRadio band ($f_{MedRadio}$), the average reflection coefficient within this first resonance bandwidth ($|S_{11}|_{@MedRadio}$), the resonance frequency around the ISM band (f_{ISM}), and the average reflection coefficient within this second resonance bandwidth ($|S_{11}|_{@ISM}$) by [–2.1%, +5.6%], [–8.2%, +35.1%], [–1.9%, +2.0%], and [–1.6%, +43.1%], respectively.

An antenna prototype is further fabricated, using photolithography (Fig. 8(b)). The reflection coefficient frequency response is measured with a VNA, and is super–imposed in Fig. 9 ("meas. / free–space"). Good agreement exists between numerical and experimental results in both the MedRadio and ISM bands. Recorded percent deviations of $f_{MedRadio}$, $|S_{11}|_{@MedRadio}$, f_{ISM}, and $|S_{11}|_{ISM}$ equal +0.2%, +1.4%, +1.1%, and +20.1%, respectively, which lie within the aforementioned expected intervals of uncertainty.

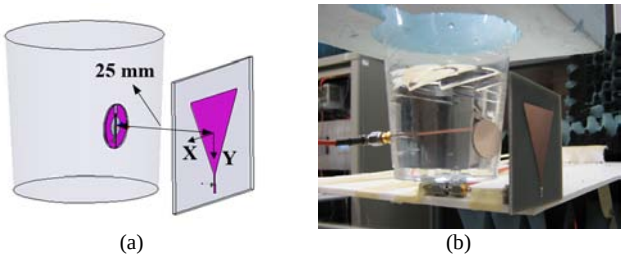

Fig. 11. (a) Numerical and (b) experimental set–ups for investigating the transmission performance between the antennas ("vertical polarization").

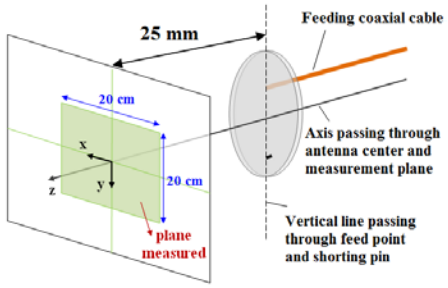

Fig. 12. Set–up for investigating the effect of misalignment between the antennas in the exhibited transmission performance (in the figure not all dimensions are in scale).

VI. Transmission Performance Investigations

A. Numerical and Experimental Set–Up

The numerical set–up used for investigating the transmission performance between the proposed implantable and on–body antennas is shown in Fig. 11(a). Origin of the coordinate system is located at the center of the on–body antenna's ground plane (Fig. 11(a)). The "to–be–fabricated antenna" design parameters are used for the implantable broadband antenna (Table II). The implantable antenna is further placed at a distance of 10 mm under the side surface of a typical drinking plastic cup, which simulates the implantation scenario of Fig. 4(b). The tissue model is assumed to be filled with dielectric material which simulates the electrical properties of the muscle–equivalent phantom formulated in Section III (ε_r = 58.0, σ = 0.8 S/m). We highlight that this tissue model has been selected because: (a) it is small in size, thus accelerating simulations, (b) it can be easily replicated experimentally, thus expediting direct inter–comparison between numerical and experimental results, (c) size and shape of the tissue model have been found to have negligible effects on the performance of implantable antennas, as long as the implantation depth remains the same [24], [38], and (d) size and shape of the tissue model have been found to not significantly affect the performance of the exterior on–body antenna, as indicated in Fig. 9 and Fig. 10, and further discussed in Section IV.B. The exterior dual–band on–body repeater antenna is placed at a distance of 15 mm outside the tissue–model, to account for the presence of human clothing in a realistic medical implantation scenario. Its ground plane faces the superstrate of the implantable antenna, which aims to favor the exterior 2400 MHz link. The simulation set–up is surrounded by free–space and absorbing boundaries.

The corresponding measurement set–up is shown in Fig. 11(b). The fabricated prototype of Fig. 3(d) accounts for the implantable antenna, which is further placed inside a typical drinking plastic cup, according to Fig. 4(b). The drinking cup is filled with the muscle–equivalent phantom that was formulated in Section III (ε_r = 58.0, σ = 0.8 S/m). The fabricated prototype of Fig. 8(b) accounts for the exterior receiving antenna of the telemetry link.

Investigations for this telemetry set–up show small deviations in the exhibited $|S_{21}|$ with rotations in polarization. As a proof concept, two polarization set–ups are hereafter investigated, i.e. "vertical polarization" (as shown in Fig. 11) and "horizontal polarization" (on–body antenna rotated by 90° around the Z axis of Fig. 11). Nevertheless, in practice, it is extremely unlikely that the link will become cross–polar. When the on–body antenna is attached to clothing, the worse that can happen is a misalignment, but little polarization mismatch is expected. To address this issue, the on–body antenna is assumed to be scanning a transversal plane at 25 mm far from the implanted antenna. Numerical and experimental investigations are carried out to assess the transmission performance in a vertical plane (20 cm × 20 cm in size), with a step of 25 mm, as shown in Fig. 12. An automated linear XY translation stage is used for the measurements. The goal is to avoid human presence in the vicinity of the antennas and uncertainty of antenna position and cable random bending.

B. Radiation Performance Investigations

The antenna radiation performance is investigated numerically, considering the simulation set–up of Fig. 11(a). Simulations are carried out at 402 MHz. Radiation efficiencies of the implantable and exterior antennas are calculated as 0.05% and 0.12%, respectively. The far–field gain radiation patterns exhibited by each of the antennas are shown in Fig. 13. The implantable broadband antenna radiates a directional radiation pattern, with its main lobe pointing out of its radiating patch. The radiation pattern of the exterior dual–band on–body antenna is a nearly omni–directional radiation pattern, as attributed to its small electrical length at the frequency under consideration (402 MHz). Maximum far–field gain values are calculated as –31.7 dBi and –27.2 dBi for the implantable and exterior antennas, respectively. For the sake of completeness, radiation performance of the exterior antenna at 2400 MHz has also been investigated. Radiation efficiency has been calculated as 34%, whereas the antenna has been found to exhibit a typical patch antenna–like far–field gain radiation pattern, with a maximum gain value of +2.1 dBi. Nevertheless, for short inter–antenna separation distances, the antennas are in the respective near field of each other. Concurrently, Fig. 14 shows the 3D polar plot of the total electric field (E_{total}) in the near–field of the antennas (radius of 25 mm, incident power of 1W). Minor changes are observed in the polar plot of Fig. 14(b) for varying phantom sizes.

C. Transmission Coefficient Investigations

Transmission coefficient (S_{21}) investigations are hereafter performed between the implantable (port 1) and on–body (port 2) antennas. The numerical and experimental set–ups used are

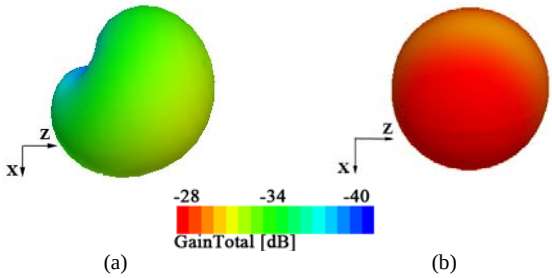

(a) (b)

Fig. 13. Far–field gain radiation patterns exhibited by the (a) implantable (coordinate system defined in Fig. 3) and (b) exterior (coordinate system defined in Fig. 8) antennas at 402 MHz, for the set–up of Fig. 11(a).

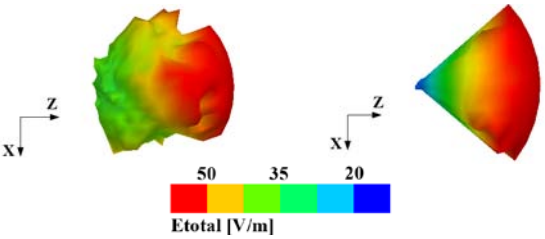

(a) (b)

Fig. 14. Polar plot of the total electric field (E_{total}) in the near–field (radius of 25 mm, incident power of 1 W) of the (a) implantable (coordinate system defined in Fig. 3) and (b) exterior (coordinate system defined in Fig. 8) antennas at 402 MHz, for the set–up of Fig. 11(a).

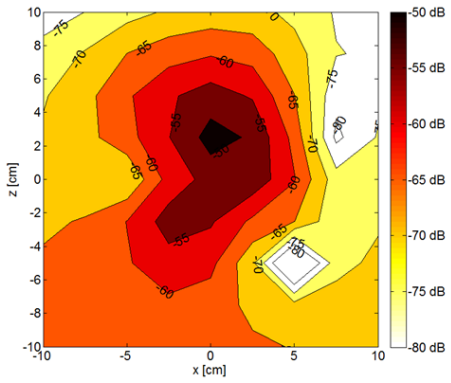

(a)

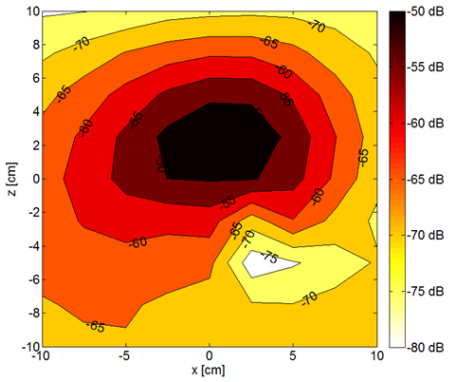

(b)

Fig. 15. Contour plots of the measured $|S_{21}|$ for various locations of the on–body antenna across the measurement plane of Fig. 12: (a) "vertical polarization", and (b) "horizontal polarization".

those depicted in Fig. 11. Fig. 15 shows contour plots of the measured $|S_{21}|$ for various locations of the on–body antenna across the measured plane of Fig. 12. Actual measurement

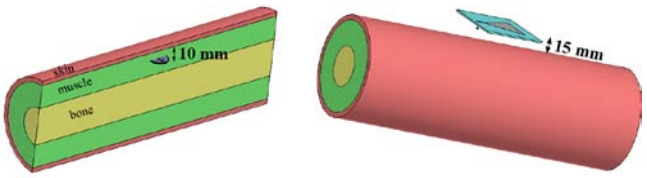

(a) (b)

Fig. 16. Realistic arm–implantation scenario: (a) implantable antenna inside arm model, (b) telemetry set–up with exterior antenna.

results are depicted in Fig. 15(a) ("vertical polarization") and Fig. 15(b) ("horizontal polarization"), which have been found to differ by less than 13.5% compared to simulations. Such deviations may be attributed to reflections by objects in the surrounding environment of the experimental set–up. Results show that reasonable misalignment of the antennas and polarization rotation are allowed within a [-5 cm, 5 cm] x [-5 cm, 5 cm] area at the expense of up to 15 dB excess attenuation in $|S_{21}|$.

In order to put the aforementioned results in a realistic perspective, further numerical investigations are carried out at 402 MHz for the implantation scenario of Fig. 16. That is, the implantable antenna is placed at a distance of 10 mm under the muscle tissue of a cylindrical three–layer (skin, muscle, bone) arm model [38], while the on–body repeater is placed at 15 mm away from it. Assuming a power of P_{Tx} available at the transmitting port (implantable antenna), then the power that is absorbed by a 50 Ohm load terminating the receiving on–body antenna, P_{Rx}, may be calculated as [20]:

$$|S_{21}|^2 = P_{Rx} / P_{Tx} \quad (1)$$

However, P_{Tx} is limited by the patient safety and EM interference regulations, as follows:

- The IEEE C95.1–1999 patient safety standard restricts the Specific Absorption Rate (SAR) averaged over any 1 g of tissue in the shape of a cube to less than 1.6 W/kg [14]. For the arm–implantation scenario, IEEE C95.1–1999 is found to restrict P_{Tx} to 5.186 mW.
- The IEEE C95.1–2005 patient safety standard restricts the SAR averaged over any 10 g of tissue in the shape of a cube to less than 2.0 W/kg [15]. For the arm–implantation scenario, IEEE C95.1–2005 is found to restrict P_{Tx} to 30.17 mW.
- To mitigate EM interference with other services taking place in the same frequency band, MedRadio regulations restrict the effective radiated power (ERP) of implantable antennas to 25 μW [39]. For the arm–implantation scenario, P_{Tx} must be restricted to 50.0 mW in order to fully meet the requirement of the ERP limitation.

Given the strictest out of the three aforementioned power limitations, P_{Tx} should be limited to less than 5.186 mW. Assuming a receiver sensitivity of –75 dBm, numerical and experimental investigations show that this amount of power can achieve a telemetry range of 60 cm between the proposed antennas. Considering the same receiver sensitivity and the antennas placed in the repeater configuration of Fig. 16, then P_{Tx} can be limited to 0.05 mW for the same telemetry range. Of course, in the latter case, another exterior antenna will be required to establish the 2400 MHz link with the on–body antenna. Aligned antennas in the "vertical polarization" set–up have been considered for these investigations. In other words, the proposed repeater configuration is found to achieve a reduction in the IMD power by a factor of 100. In this case, patient safety and EM interference performance of the implantable antenna are far below the regulatory limits, while lifetime of the IMD may be considerably increased. If the maximum allowable power level is delivered to the implantable antenna in this repeater configuration, then successful data telemetry may be achieved even if the on–body antenna is cross–polarized and deviated by 10 cm from its original position. Even lower P_{Tx} values can be achieved for higher–sensitivity receivers. For example, a receiver sensitivity of –116 dBm may be achieved by the Texas Instruments (TI) CC1101 transceiver module [40] for 0.6 kBaud transmission of Gaussian Frequency Shift Keying (GFSK) modulated data.

VII. Conclusion

In this paper, we designed and tested a novel MedRadio antenna for muscle–implantation, as well as a novel on–body antenna for operation in the MedRadio and ISM bands. The idea is to integrate these antennas into IMDs and on–body repeaters, respectively. The repeater will be placed at a close distance to the low–efficiency IMD to receive its transmitted data (MedRadio band), and re–transmit them to exterior devices placed further apart (ISM band). The advantage of this relay approach is that it reduces power consumption in the IMD, and extends its battery life. Compared to previous designs, the proposed implantable antenna shows improved tolerance to detuning, by exhibiting an enhanced BW_{15dB} (66 MHz), further to its BW_{10dB} (87 MHz). Emphasis is given in preserving patient comfort, by introducing circular shape to avoid sharp edges, and miniaturizing its size (399 mm^3). The proposed on–body antenna is one of the very few designs appearing in the literature for dual–operation in the MedRadio and ISM bands.

The transmission performance between these antennas was further investigated. Results indicated that the power delivered to the implantable antenna may be limited to as low as 0.05 mW for a typical arm implantation scenario, and an on–body receiver sensitivity of –75 dBm. For comparison, the maximum telemetry range that could be achieved for these antennas in a non–repeater configuration (60 cm) would require a delivered power of 5.186 mW. Therefore, using the proposed configuration, patient safety and EM interference performance of the implantable antenna are far beyond the regulatory limitations. Even lower power levels may be achieved for higher–sensitivity receivers. Further investigations demonstrated that the exhibited transmission performance is nearly insensitive to slight misalignment and polarization rotation of the antennas.

Overall, a repeater configuration approach was proposed for IMDs, and proved to be feasible, enabling reduction of the IMD power by a factor of 100 for acquiring the maximum telemetry range that could be achieved without the repeater configuration. At the same time, small size factor was

maintained for the implantable and repeater antennas, while the configuration was shown to exhibit robustness to uncertainties inherent to the relative positioning of the antennas.

ACKNOWLEDGEMENT

The authors would like to gratefully thank C. Brito and A. Almeida from Instituto Superior Técnico, Lisbon, Portugal, for prototype fabrication and measurements.

REFERENCES

[1] C.J. Sanchez–Fernandez, O. Quevedo–Teruel, J. Requena–Carrion, L. Inclan–Sanchez, E. Rajo–Iglesias, "Dual–band microstrip patch antenna based on short–circuited ring and spiral resonators for implantable medical devices," IET Microw. Antennas Propag., vol. 4, pp. 1048–1055, Aug. 2010.

[2] M.L. Scarpello, D. Kurup, D. Vande Ginste, F. Axisa, J. Vanfleteren, W. Joseph, L. Martens, and G. Vermeeren, "Design of an implantable slot dipole conformal flexible antenna for biomedical applications," *IEEE Trans. Antennas Propag.*, vol. 59, pp. 3556 – 3564, Oct. 2011.

[3] Z. Noroozi and F. Hojjat–Kashani, "Three–dimensional FDTD analysis of the dual–band implantable antenna for continuous glucose monitoring," *Prog. Electrom. Res. Lett.*, vol. 28, pp. 9–21, 2012.

[4] FCC, Washington, DC, USA, "Federal Communications Commission," 2012 [Online]. Available: http://www.fcc.gov

[5] A. Kiourti and K.S. Nikita, "Numerical assessment of the performance of a scalp-implantable antenna: Effects of head anatomy and dielectric parameters," *Wiley Bioelectrom.*, vol. 34, pp. 167–179, Apr. 2013.

[6] A. Kiourti and K.S. Nikita, "Miniature scalp-implantable antennas for telemetry in the MICS and ISM bands: Design, safety considerations and link budget analysis," IEEE *Trans. Antennas Propag.*, vol. 60, pp. 3568–3575, Aug. 2012.

[7] T. Karacolak, A.Z. Hood, and E. Topsakal, "Design of a dual–band implantable antenna and development of skin mimicking gels for continuous glucose monitoring," *IEEE Trans. Microw. Theory Techn.*, vol. 56, pp. 1001–1008, Apr. 2008

[8] C.M. Lee, T.C. Yo, F.J. Huang, and C.H. Luo, "Bandwidth enhancement of planar inverted–F antenna for implantable biotelemetry," *Microw. Opt. Technol. Lett.*, vol. 51, pp. 749–752, Mar. 2009.

[9] W.C. Liu, S.H. Chen, and C.M. Wu, "Bandwidth enhancement and size reduction of an implantable PIFA antenna for biotelemetry devices," *Microw. Opt. Technol. Lett.*, vol. 51, pp. 755–757, Mar. 2009.

[10] H. Higgins, "In–body RF communications and the future of healthcare," Zarlink Semiconductor [Online]. Available: http://www.armms.org/media/uploads/1128506900.pdf

[11] F. Merli, L. Bolomey, J.F. Zurcher, G. Corradini, E. Meurville, and A.K. Skrivervik, "Design, realization and measurements of a miniature antenna for implantable wireless communication systems," *IEEE Trans. Antennas Propag.*, vol. 59, pp. 3544 – 3555, Oct. 2011.

[12] P. M. Izdebski, H. Rajagopalan, and Y. Rahmat-Samii, "Conformal ingestible capsule antenna: A novel chandelier meandered design," *IEEE Trans. Antennas Propag.*, vol. 57, no. 4, pp. 900–909, Apr. 2009.

[13] A.K. Skrivervik, "Implantable antennas: the challenge of efficiency," in *Proc. Europ. Conf. Antennas Propag.*, Gothenburg, 2013, pp. 3516–3520.

[14] *IEEE Standard for Safety Levels With Respect to Human Exposure to Radiofrequency Electromagnetic Fields, 3 kHz to 300 GHz*, IEEE Standard C95.1, 1999.

[15] *IEEE Standard for Safety Levels With Respect to Human Exposure to Radiofrequency Electromagnetic Fields, 3 kHz to 300 GHz*, IEEE Standard C95.1, 2005

[16] J. Kim and Y. Rahmat-Samii, "Implanted antennas inside a human body: Simulations, designs and characterizations," *IEEE Trans. Microw. Theory Tech.*, vol. 52, pp. 1934–1943, Aug. 2005.

[17] F. Merli, L. Bolomey, F. Gorostidi, B. Fuchs, J.F. Zurcher, Y. Barrandon, E. Meurville, J.R. Mosig, and A.K. Skrivervik, "Example of data telemetry for biomedical applications: an in vivo experiment," *IEEE Antennas Wireless Propag. Lett.*, vol. 11, pp. 1650–1654, 2012.

[18] T. Houzen, M. Takahashi, and K. Ito, "Implanted antenna for an artificial cardiac pacemaker system," in *Prog. Electrom. Res. Symp.*, Prague, 2007, pp. 51–54.

[19] Z.N. Chen, G.C. Liu, and T.S.P. See, "Transmission of RF signals between MICS loop antennas in free space and implanted in the human head," *IEEE Trans. Antennas Propag.*, vol. 57, pp. 1850–1853, Jun. 2009.

[20] R. Warty, M.-R. Tofighi, U. Kawoos, and A. Rosen, "Characterization of implantable antennas for intracranial pressure monitoring: Reflection by and transmission through a scalp phantom," *IEEE Trans. Microw. Theory Tech.*, vol. 56, pp. 2366–2376, Oct. 2008.

[21] "International Telecommunications Union-Radiocommunications (ITU-R), radio regulations, section 5.138 and 5.150," ITU. Geneva, Switzerland, [Online]. Available: [Online]. Available: http://itu.int/home

[22] K. Kwon, J. Ha, S. Lee, and J. Choi, "Design of a dual–band on–body antenna for a wireless body area network repeater system," *Hindawi Int. J. Antennas Propag.*, vol. 2012, pp. 1–5, 2012.

[23] *Ansoft High Frequency Structure Simulator (HFSS)*, Ver. 11, Ansoft Corporation, Pittsburgh, PA, 2008.

[24] A. Kiourti and K.S. Nikita, "Accelerated design of optimized implantable antennas for medical telemetry," *IEEE Antennas Wireless Propag. Lett.*, vol. 11, pp. 1655–1658, 2012.

[25] P. S. Hall and Y. Hao, Antennas and Propagation for Body-centric Wireless Communications. Norwood, MA, USA: Artech House, 2006, ch. 9.

[26] T. Yilmaz, T. Karacolak, and E. Topsakal, "Characterization of muscle and fat mimicking gels at MICS and ISM bands (402–405 MHz and 2.40–2.48 GHz)," in *Proc. XXIX Gen. Ass. Int. Union Rad. Sc.*, 2008.

[27] A. Kiourti, J.R. Costa, C.A. Fernandes, A.G. Santiago, and K.S. Nikita, "Miniature implantable antennas for biomedical telemetry: from simulation to realization," *IEEE Trans. Biomed. Eng.*, vol. 59, pp. 3140–3147, Nov. 2012.

[28] D. Berube, F.M. Ghannouchi, and P. Savard, "A comparative study of four open-ended coaxial probe models for permittivity measurements of lossy dielectric/biological materials at microwave frequencies," *IEEE Trans. Microw. Theory Techn.*, vol. 44, pp. 1928–1934, 1996.

[29] Rohde & Schwarz Application Note RAC0607-0019, "Measurement of dielectric material properties," 2012.

[30] S. Salman, D. Psychoudakis, and J.L. Volakis, "Determining the relative permittivity of deep embedded biological tissues," *IEEE Antennas Wireless Propag. Lett.*, vol. 11, pp. 1694–1697, 2012.

[31] C. Gabriel, S. Gabriel, and E. Corthout, "The dielectric properties of biological tissues," *Phys. Med. Biol.*, vol. 41, pp. 2231–2293, 1996.

[32] A. Kiourti and K.S. Nikita, "Miniaturization vs gain and safety considerations of implantable antennas for wireless biotelemetry," in *Proc. Int. Conf. Antennas Propag.*, Chicago, IL, 2012.

[33] A. Kiourti and K.S. Nikita, "A review of implantable patch antennas for biomedical telemetry: challenges and solutions," *IEEE Antennas Propag. Mag.*, vol. 54, pp. 210–228, Jun. 2012.

[34] J. Abadia, F. Merli, J.–F. Zürcher, J.R. Mosig, and A.K. Skrivervik, "3D–spiral small antenna design and realization for biomedical telemetry in the MICS band," *Radioeng.*, vol. 18, pp. 359–367, Dec. 2009.

[35] W. W. Capello, J. D'Anthonio, J. Feinberg, and M. Manley, "Alternative bearing surfaces: alumina ceramic bearings for total hip arthroplasty," in *Bioceram Alt Bear in Joint Arthroplasty*, Session 3, Eds. Springer, 2005, pp. 87–94.

[36] F. Merli, L. Bolomey, J.-F. Zürcher, E. Meurville, and A.K. Skrivervik, "Versatility and tunability of an implantable antenna for telemedicine," in *Proc. 5th European Conference on Antennas and Propagation (EuCAP 2011)*, Rome, Italy, 2011.

[37] F. Merli and A. K. Skrivervik, "Design and measurement considerations for implantable antennas for telemetry applications," in Proc. *Europ. Conf. Antennas Propag.*, Barcelona, 2010, pp. 1–5.

[38] A. Kiourti and K.S. Nikita, "Detuning issues and performance of a novel implantable antenna for telemetry applications," in *Proc. Europ. Conf. Antennas Propag.*, Prague, 2012, pp. 746–749.

[39] Recommendation ITU-R SA.1346. Geneva, Switzerland, 1998, Int. Telecommun. Union.

[40] Texas Instruments. CC1101 Evaluation Module 433 MHz [Online]. Available: http://www.ti.com/tool/cc1101emk433

Asimina Kiourti (S'10, M'14) received the Diploma in Electrical and Computer Engineering from the University of Patras, Greece (2008), the MSc in Technologies for Broadband Communications from University College London, U.K. (2009), and the PhD degree in Electrical and Computer Engineering from the National Technical University of Athens, Greece (2013).

Dr. Kiourti is currently a Postdoctoral Researcher at the ElectroScience Laboratory of The Ohio State University. She has authored or co-authored more than 40 journal and conference papers and 4 book chapters. Her research interests include antennas for medical applications, medical sensing, RF circuits, bioelectromagnetics, and flexible textile and polymer-based antennas.

Dr. Kiourti has received various awards and scholarships, among which, the IEEE MTT-S Graduate Fellowship for Medical Applications for 2012 and the IEEE AP-S Doctoral Research Award for 2011. She is a member of the Technical Chamber of Greece and the IEEE.

Jorge R. Costa (S'97–M'03–SM'09) was born in Lisbon, Portugal, in 1974. He received the Licenciado and Ph.D. degrees in electrical and computer engineering from the Instituto Superior Técnico (IST), Technical University of Lisbon, Lisbon, Portugal, in 1997 and 2002, respectively.

He is currently a Researcher at the Instituto de Telecomunicações, Lisbon, Portugal. He is also an Associate Professor at the Departamento de Ciências e Tecnologias da Informação, Instituto Universitário de Lisboa (ISCTE-IUL). His present research interests include lenses, reconfigurable antennas, implantable antennas, MEMS switches, UWB, MIMO and RFID antennas. He is the coauthor of four patent applications and more than 100 contributions to peer reviewed journals and international conference proceedings. More than twenty of these papers have appeared in IEEE Journals.

Prof. Costa is currently serving as an Associate Editor for the IEEE TRANSACTIONS ON ANTENNAS AND PROPAGATION and he was a Guest Editor of the Special Issue on "Antennas and Propagation at mm- and Sub mm-Waves", from the IEEE TRANSACTIONS ON ANTENNAS AND PROPAGATION, April 2013.

Carlos A. Fernandes (S'86–M'89–SM'08) received the Licenciado, M.Sc., and Ph.D. degrees in electrical and computer engineering from Instituto Superior Técnico (IST), Technical University of Lisbon, Lisbon, Portugal, in 1980, 1985, and 1990, respectively.

He joined IST in 1980, where he is presently Full Professor at the Department of Electrical and Computer Engineering in the areas of microwaves, radio wave propagation and antennas. He is a Senior Researcher at the Instituto de Telecomunicações and member of the Board of Directors. He has been the leader of antenna activities in National and European Projects as RACE 2067-MBS (Mobile Broadband System), ACTS AC230-SAMBA (System for Advanced Mobile Broadband Applications) and ESA/ESTEC-ILASH (Integrated Lens Antenna Shaping). He has coauthored a book, a book chapter, and more than 130 technical papers in peer reviewed international journals and conference proceedings, in the areas of antennas and radiowave propagation modeling. His current research interests include dielectric antennas for millimeter wave applications, antennas and propagation modeling for personal communication systems, RFID antennas, artificial dielectrics and metamaterials. He was a Guest Editor of the Special Issue on "Antennas and Propagation at mm- and Sub mm-Waves", from the IEEE Transactions on Antennas and Propagation, 2013.

Konstantina S. Nikita (M'96–SM'00) received the Diploma (1986) in Electrical Engineering and the Ph.D. degree (1990) from the National Technical University of Athens (NTUA), as well as the M.D. degree (1993) from the Medical School, University of Athens.

From 1990 to 1996, she worked as a Researcher at the Institute of Communication and Computer Systems. In 1996, she joined the School of Electrical and Computer Engineering, NTUA, as an Assistant Professor, and since 2005 she serves as a Professor at the same School. She has authored or co-authored 165 papers in refereed international journals and chapters in books, and over 300 papers in international conference proceedings. She is editor of four books in English, and author of two books in Greek. She holds two patents. She has been the technical manager of several European and National R&D projects. She has been honorary chair/ chair of the program/organizing committee of several international conferences and she has served as keynote/invited speaker at international conferences, symposia and workshops organized by NATO, WHO, ICNIRP, IEEE, URSI, COMCON, PIERS etc. She has been the advisor of 22 completed Ph.D. theses, several of which have received various awards. Her current research interests include biological effects and medical applications of radiofrequency electromagnetic fields, biomedical signal and image processing and analysis, simulation of physiological systems, and biomedical informatics.

Dr Nikita is Associate Editor of the IEEE Transactions on Biomedical Engineering, the IEEE Journal on Biomedical and Health Informatics, the Wiley-Bioelectromagnetics and guest editor of several international journals. She has received various honors/awards, among which, the Bodossakis Foundation Academic Prize (2003) for exceptional achievements in "Theory and Applications of Information Technology in Medicine". She has been a member of the Board of Directors of the Atomic Energy Commission, of the Hellenic National Academic Recognition and Information Center, and of the Hellenic National Council of Research and Technology. She has also served as deputy head of the School of Electrical and Computer Engineering of the NTUA. She is a member of the Hellenic National Ethics Committee, a Founding Fellow of the European Association of Medical and Biological Engineering and Science (EAMBES), a member of the Technical Chamber of Greece and of the Athens Medical Association. She is also the founding chair and ambassador of the IEEE-EMBS, Greece chapter and vice chair of the IEEE Greece Section.